RECEIVE

REPORT DOCUMENTATION PAGE

AFRL-SR-AR-TR-03-

0343

1. REPORT DATE (25-2-2003)	2. REPORT TYPE	3. DATES COVERED (From - To) 7/1/2002 to 6/30/2003

4. TITLE AND SUBTITLE

Measurement of Stress in Ceramic Laminates with Micro-Raman

5a. CONTRACT NUMBER

5b. GRANT NUMBER F49620-02-10340

5c. PROGRAM ELEMENT NUMBER

6. AUTHOR(S)

Nina Orlovskaya

5d. PROJECT NUMBER 020890

5e. TASK NUMBER

5f. WORK UNIT NUMBER

7. PERFORMING ORGANIZATION NAME(S) AND ADDRESS(ES)

Drexel University
Philadelphia, PA 19104

8. PERFORMING ORGANIZATION REPORT NUMBER

9. SPONSORING / MONITORING AGENCY NAME(S) AND ADDRESS(ES)

10. SPONSOR/MONITOR'S ACRONYM(S)

11. SPONSOR/MONITOR'S REPORT NUMBER(S)

12. DISTRIBUTION / AVAILABILITY STATEMENT

Approved for public release. Distribution is unlimited

20030915 008

13. SUPPLEMENTARY NOTES

14. ABSTRACT

Residual stresses in laminate ceramic composites were measured by micro-Raman spectroscopy. The research proceeded from laminate samples preparation, which included mixture of powders in certain proportion, grinding them up to submicron dispersity, rolling of the tapes, placing the tapes in certain order and hot pressing. Several different ceramic laminates, such as Ti3SiC2-ZrO_2, B_4C-SiC, and Si_3N_4-TiN, were used for the determination of residual stresses by micro-Raman. The $AlMgB_{14}$-TiB_2 superhard laminates are being prepared by SHS powder synthesis and hot pressing. The residual stresses in Ti3SiC2 based laminates were not significant, because of the small mismatch in CTEs of Ti3SiC2 and ZrO2. In B4C-SiC laminates, residual stresses could be measured from the shift of transverse optic (TO, 790cm-1) and longitudinal optic (LO, 973cm-1) phonon modes. In silicon nitride based laminates several Raman bands could be used for the determination of the surface residual stresses.

15. SUBJECT TERMS

16. SECURITY CLASSIFICATION OF:			17. LIMITATION OF ABSTRACT	18. NUMBER OF PAGES	19a. NAME OF RESPONSIBLE PERSON
a. REPORT	b. ABSTRACT	c. THIS PAGE		8	Nina Orlovskaya
					19b. TELEPHONE NUMBER (include area code) 215-895-1541

Status of Effort:

The control over the mechanical behavior and reliability of laminates can be obtained only through design, measurements of residual stresses and their redistribution during loading in laminate materials. The sign and value of surface and bulk residual stresses have to be firmly established by experimental measurements and theoretical prediction. Thus, there exists a theoretical background that allows for the design of laminated ceramics. There are also a number of experimental studies of laminated ceramics that were conducted using these models, attempting to maximize the mechanical properties. However, it is impossible to predict whether the utilized approach of developing internal stresses will be successful if the stress in the layers has not been measured with a high spatial resolution.

The goal of the work is to study the interrelation between manufacturing, structure, and residual stresses of complex particulate-layered Ti_3SiC_2-ZrO_2, B_4C-SiC, $AlMgB_{14}$-TiB_2, and Si_3N_4 based composites. Micro-Raman spectroscopy was used to measure residual stresses in separate layers of ceramic laminates.

Accomplishments/New Findings:

Laminate design for enhanced K_{Ic}

In case of non-homogeneous (particularly, layered) materials, so-called apparent fracture toughness should be considered. This is the fracture toughness of an equivalent homogeneous specimen. If we measure fracture toughness in bending, the effective sample parameters should satisfy the following conditions: 1) the homogeneous specimen has to have the same dimensions as the layered specimen; 2) the homogeneous specimen has a notch depth equal to that of the layered specimen; 3) under the same loading conditions the homogeneous specimen has to demonstrate the same load to fracture as the layered specimen. Under these considerations the apparent fracture toughness is the fracture toughness calculated from test data of the layered sample considering this specimen as "homogeneous". Such an approach does not meet the fracture mechanics requirement of taking into account all features of stress distribution near the crack tip in layered media, but it is still a useful characteristic allowing an effective contribution of such factors as residual stresses and material inhomogeneity to be accounted for.

The compressive residual stress σ_r in the outside layers of a laminate shields natural and artificial cracks in the layer. Therefore, the effective (apparent) fracture toughness of such a structure increases. The more compressive the residual stress induced, the more shielding occurs. Another important factor that contributes to the apparent fracture toughness increase is the crack length a. A longer crack promotes more shielding. The maximum length of a transverse crack in an outside compressive layer is limited by the layer thickness l_l. These two factors determine the apparent fracture toughness of the material.

In general, the condition for crack growth onset is

$$K_a+K_r=K_c \qquad (1)$$

(Fig. 1), where $K_a=K_a(\sigma_a, a)$ is the applied stress intensity factor that can be measured, σ_a is the distribution of applied stress resulting from bending, $K_r=K_r(\sigma_r, a)$ is the stress intensity factor due to residual stress σ_r, and K_c is the intrinsic fracture toughness of the material in the layer. If a condition of a crack growth onset is fulfilled then $K_a=K_c-K_r$ is the apparent fracture toughness. If σ_r is compressive, then $K_r<0$ and K_a increases. The more $|\sigma_r|$, the more the K_a.. The more the a, the more K_a.. The largest value of a crack length in compressed layer is l_l. The maximum apparent fracture toughness can be obtained for such crack. Unfortunately, small cracks have K_a close to K_c.

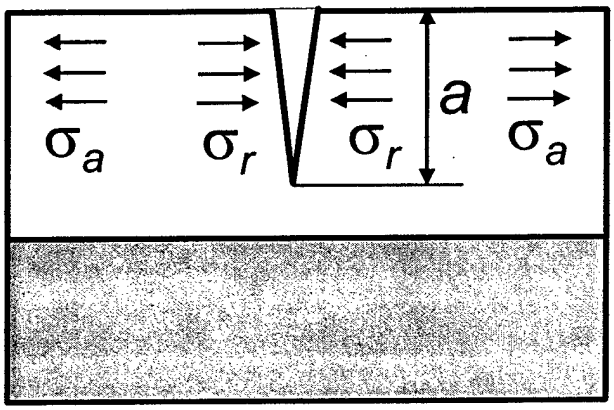

Fig. 1. A schematic presentation of the condition of the crack growth onset.

The design technique to obtain the enhanced fracture toughness of a layered composite is as follows. First, the compositions of the layers are selected depending on the intended application of the composite. Then, the relevant material constants entering the design are determined. The constants for design are the coefficient of thermal expansion, Young's modulus, Poisson's ratio, and the density of the corresponding constituents. A very important but experimentally unknown parameter is ΔT – a "joining" temperature. Further, effective coefficients of thermal expansion, effective Young's modulus, average density and the thickness ratio of layers are determined using the rule of mixture. The next step in the design is the selection number of the layers. It can be any appropriate number depending on the required total thickness of the tile. To obtain the enhanced fracture resistance of the layered composite, the factors affecting the apparent fracture toughness should be taken into account. Usually, the thickness of the thinnest possible layer is limited by the manufacturing technology. Note that a compressive layer should be thin enough to reach a high level of residual stress. Another important requirement is the thickness ratio of layers with high CTE (a tensile stress) and layers with lower CTE (a compressive stress). Any appropriate thickness ratio can be used as a first approximation. Then the ensile layer thickness is found. After this, the calculation of residual stresses is done using (1) and (2). The total thickness of the sample is also determined at this step for a given layer's thickness ratio taking into account the selected number of layers. The thickness ratio is changed after analysis of the residual stress and the total thickness of the specimen. Note that increasing the ratio of tensile layer thickness to compressive layer thickness decreases tensile residual stress. However, it can result in increasing total thickness of sample. After changing thickness ratio, the calculation is repeated. Such iterations are continued to find a unique optimal layer thickness ratio that produces the maximum possible compressive residual stress, low tensile residual stress, and necessary total thickness of the sample. The maximum possible apparent fracture toughness of the corresponding layered structure is also determined in all iterations as an indicative parameter of the design (Table 2). The determination of the apparent K_{Ic} uses the compressive residual stress and the thickness of an outside layer as a crack length at any given iteration. These two parameters (the compressive residual stress and the thickness of the top layer) have trends acting in opposite directions. A decrease in the top layer thickness can increase the residual stress in the layer, but it decreases the length of the maximum crack. Therefore, the maximum apparent fracture toughness was always used to analyze the correct thickness ratio.

The schematic presentation of symmetric three-layered composite that was considered for design and manufacturing is shown in Fig.2. The proposed design targeted a fracture toughness increase of B_4C-SiC composites and was based on the preliminary results both from our work and from the work of others. The material systems selected for the proposed study were B_4C and B_4C-30wt%SiC because of their promise for ballistic applications. Table 1 shows the relevant material constants entering the design (compiled from the literature), and Table 2 shows the corresponding calculated residual stresses in the B_4C/B_4C-30wt%SiC laminates. The maximum possible apparent fracture toughness for corresponding layered structures is also presented. The layers under tensile stress have higher CTE, and in this case they are B_4C layers. The layers under compressive stress have lower CTE; here they are B_4C-30wt%SiC layers. A temperature T= 2150°C was used for the majority of the calculations, when residual stresses appeared in the layers upon cooling from the hot pressing temperature. There is no liquid phase present during the sintering of B_4C/B_4C-SiC ceramics,

therefore, the hot pressing temperature was used as a "joining" temperature ΔT for calculations. All laminates were designed in such a way that the tensile stresses had been maintained at low values. It should be noted the value of K_{Ic} given in the Table 2 is the apparent fracture toughness that was used to estimate the maximum possible toughening of the 3 layered laminate. The experimental values measured using Single Edge V Notch Beam (SEVNB) method yielded 7.42±0.82 MPa.m$^{1/2}$, which is still a very high value for brittle boron carbide based composites.

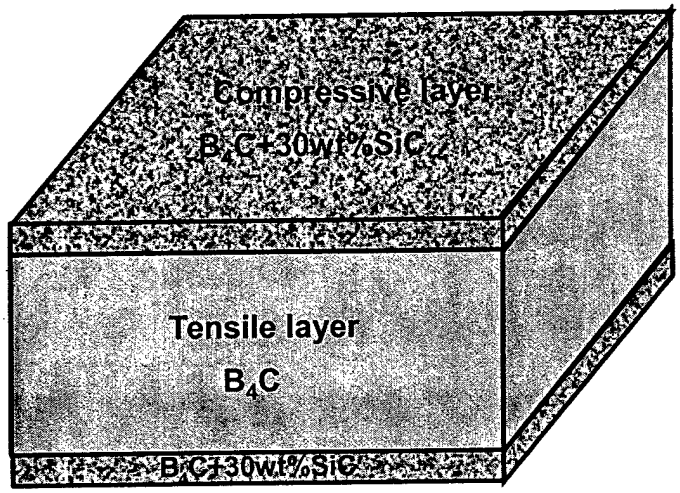

Fig. 2. Schematic presentation of symmetric 3 layered composite

Table 1. Properties of ceramics used in the stress calculation

Composition	***E, GPa***	***Poisson's ratio***	CTE, 10^{-6} K^{-1}
B_4C	483	0.17	5.5
SiC	411	0.16	3

Table 2. Three layered composite design. The total thickness of a tile – 10.5mm

Thickness of Layers, μm		σ_{comp}, MPa	σ_{tens}, MPa	Apparent K_{Ic}, MPa.m$^{1/2}$
B_4C-30wt%SiC	B_4C			
900	8700	632	131	44

The microstructure of pure B_4C layer of 3 layered B_4C-B_4C-30wt%SiC laminate with 4% of porosity is presented in Fig. 3. As one can see, the porosity exists at the grain boundary of the ceramics that might be a reason that three layered laminates have not outperformed the dense monolithic boron carbide tiles. A different set of ballistic experiments are required where fully dense boron carbide based laminates will be used for comparison. Such experiments will be performed in future. While no 3 layered composite material was possible to collect after the penetration tests, in a separate ballistic test designed specifically at low projectile velocity the debris of 3 layered comminuted composite was collected to study the microstructural changes in material after ballistic impact. The size of the comminuted particles collected after impact varied from 5-10 μm to 1-2 mm. The density of this tile was very close to the theoretical density of the material, therefore we could consider that the tile was almost fully dense. While a separate paper will be prepared with detailed results of the microstructural study of comminuted B_4C and B_4C-30wt%SiC ceramics, some specific features of fractured ceramics are shown here in Fig. 4 and 5.

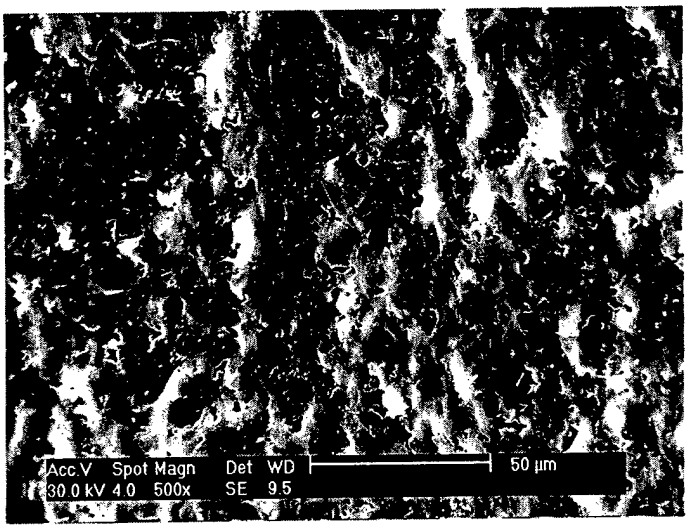

Fig. 3. The microstructure of pure B_4C layer in 3 layered B_4C/B_4C-30wt%B_4C composite.

The microstructure of the pure B_4C layer comminuted by ballistic impact is shown in Fig. 4. The smooth and flat surface with transgranular fracture was typically observed for B_4C layers with some amount of cleavage steps present in the material. Such cleavage mode plays an important role both in fracture and in the fragmentation event during ballistic impact. There was always some amount of closed porosity which was not possible to eliminate by any special treatment such as increase of hot pressing temperature, pressure or a dwell time increase.

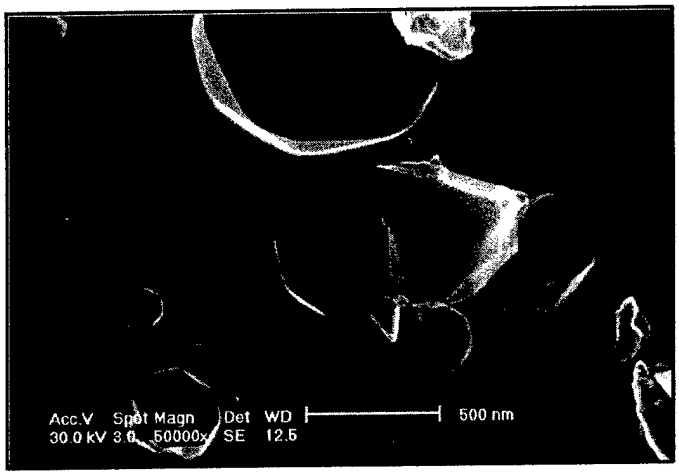

Fig. 4. Micrograph of a B_4C grain in the pure boron carbide layer of the 3 layered laminate. Closed porosities were present.

The microstructure of the B_4C-30wt%SiC layer after impact is shown in Fig.5. The B_4C grains are still fractured almost always transgranularly, and a small amount of closed porosity was present in boron carbide grains. All SiC grains fracture surfaces was heavily cleaved with almost no grains observed without cleavage. Such ability of the material to form shear or cleavage steps should significantly increase the resistance to penetration of SiC ceramic composites. This is a topic for further intensive research, however what is clear at the moment that B_4C and SiC have distinctively different deformation modes under ballistic impact.

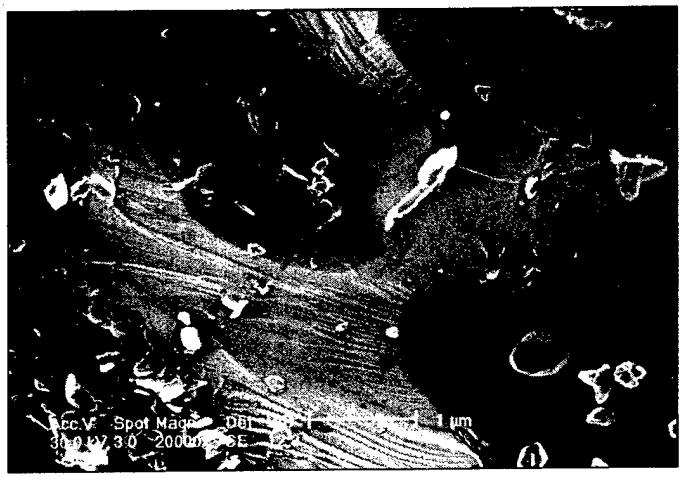

Fig. 5. Micrograph of the B_4C-30wt%SiC layer of the 3 layered laminate. The closed porosity was present in a number of B_4C grains. Almost all SiC grains have been heavily cleaved

Analysis of residual stresses

In this research the two-component brittle layered composites with symmetric macrostructure are considered. The layers consisting of different components alternate one after another, but the external layers consist of the same component. Thus the total number of layers N in such a composite sample is odd. The layers of the first component including two external (top) layers are designated by index 1 (j = 1), and the layers of the second component (internal) are designated by index 2 (j = 2). The number of layers designated by index 1 is $(N+1)/2$ and the number of layers designated by index 2 is $(N-1)/2$. The layer of each component has some constant thickness, and the layers of same component have identical thickness. The properties of the materials used in the calculation are given in Table 1.

Table 3. Young's moduli and CTE of the components

Composition	**E, GPa**	**CTE, 1/K**
Si_3N_4 - 5wt% Y_2O_3 - 2wt% Al_2O_3	320	$3x10^{-6}$
TiN	440	$9.35x10^{-6}$
Si_3N_4 (5wt% Y_2O_3 - 2wt% Al_2O_3) - 20wt% TiN	335.62	$3.826x10^{-6}$
Si_3N_4 (5wt% Y_2O_3 - 2wt% Al_2O_3) - 50wt% TiN	364.93	$5.378x10^{-6}$

There are effective residual stresses in the layers of each component in the layered ceramic composite. During cooling, the difference in deformation, due to the different thermal expansion factors of the components, is accommodated by creep as long as the temperature is high enough. Below a certain temperature, which is called the "joining" temperature, the different components become bonded together and internal stresses appear. In each layer, the total strain after sintering is the sum of an elastic component and of a thermal component . The residual stresses in the case of a perfectly rigid bonding between the layers of a two-component material are:

$$\sigma_{r1} = \frac{E_1' E_2' f_2 (\alpha_{T2} - \alpha_{T1}) \Delta T}{E_1' f_1 + E_2' f_2} \qquad (2)$$

and

$$\sigma_{r2} = \frac{E_2' E_1' f_1 (\alpha_{T1} - \alpha_{T2}) \Delta T}{E_1' f_1 + E_2' f_2}, \qquad (3)$$

where $E_j' = E_j / (1 - \nu_j)$, $f_1 = \frac{(N+1)l_1}{2h}$, $f_2 = \frac{(N-1)l_2}{2h}$, E_j and ν_j is the elastic modulus and Poisson's ratio of j-th component respectively, l_1 and l_2 are the thickness of layers of the first and second component,

α_{T1} and α_{T2} are the thermal expansion coefficients (CTE) of the first and second components respectively, ΔT is the difference in temperature of joining temperature and current temperature, h is the total thickness of the specimen.

Equations (2) and (3) give the residual stresses in layers which have an infinitive extent. Far away from the free surface, the residual stress in the layer is uniform and equibiaxial. In the bulk of layers the stress perpendicular to the layers is zero. At the free surface of the laminates the stresses are different from the bulk stresses. Near the edges the residual stress state is not equibiaxial because the edges themselves must be traction-free. Highly localized stress components perpendicular to the layer plane exist near the free surface and it is decreasing rapidly from the surface becoming negligible at a distance approximately on the order of the layer thickness. These stresses have a sign opposite to that of the equibiaxial stresses deep within the layer. Therefore, if the bulk stress is compressive within material, the tensile stress components appear at or near the free surface of a layer.

Measurement of residual stresses is a critical issue in the development of composites. It is important for improvement of the mechanical performance of the composite. In practice the residual stresses in laminates are determined usually by not only the thermoelastic parameters mismatch but also different stress relaxation processes in layer microstructure. The microstructure is modified by technology. Therefore there is no exact initial knowledge of layer properties and layer mechanical behavior. Consequently there is no possibility to calculate real residual stress precisely. In many cases the spatial distribution of residual stresses in layers is very important to obtain desirable mechanical behavior of composite. Techniques that have the capability to map stress distributions (i.e., to measure the absolute magnitude of the stress at different points within the material) would represent an important advance in the evaluation of the mechanical properties that are relevant to real world applications. A range of different methods, such as X-ray and neutron diffraction, strain-curvature measurements, chemical etching and others, are currently available for the estimation of residual stresses. For each of these methods of stress determination there are a number of restrictions. These include measurement accuracy, spatial resolution, ease of measurements and applicability to different materials.

In recent years the stress analysis of ceramics using so called piezo-spectroscopic techniques including Raman spectroscopy, has been reported. Strengthening contribution arising from the residual stresses in Al_2O_3/ZrO_2 composites has been evaluated. The magnitude of bridging stresses in Si_3N_4 and Al_2O_3 during crack propagation was estimated, and some attempts to use Raman spectroscopy to estimate the residual stresses around indentation in silicon nitride have been done, but the results were contradictive and further clarification is needed. This analysis is based on the measurements of a peak shift of Raman band when the material is subjected to a stress field. The frequency shift of the Raman bands is proportional to the mean stress averaged over the volume of the probed material. This is usually referred to as the piezo-spectroscopic effect. The piezo-spectroscopic effect for polycrystalline materials can be expressed by the following equation:

$$\Delta\nu = \Pi < \sigma_{jj} > \qquad (4)$$

where $\Delta\nu$ is the observed frequency shift from the unstressed state, σ_{jj} is the stress component expressed with the Repeated Index Notation ($\sigma_{jj} = \sigma_{11} + \sigma_{22} + \sigma_{33}$), the brackets $< >$ refer to the spatial average and Π is the piezo-spectroscopic coefficient. This coefficient is obtained by means of an appropriate calibration, whereby known stresses are applied to the polycrystalline material and the resulting frequency shifts are recorded: for small stresses (up to several hundred MPa) the dependence is usually linear and the least square fit to these data provides the piezo-spectroscopic coefficients. Once the piezo-spectroscopic coefficient has been determined, then an observed frequency shift can be converted directly to stress. It should be noted that the mean stress is derived from $\sigma_{mean} = \sigma_{jj}/3 = (\sigma_{11} + \sigma_{22} + \sigma_{33})/3$. In such a way the mean stress can be found from (4).

In Si_3N_4 layers, due to the thermal mismatch between layers, the shift reflects the sum of residual stresses in layer and edge stress components due to probing of near-surface volumes. To separate the mean stress contribution from the total measured stress, including microstresses in different grains and particles, it is necessary to measure the band positions in virgin Si_3N_4 ceramics without the constraint of laminating. By subtracting the virgin frequency from that of the layered material we can calculate the mean stress by lamination in the Si_3N_4 layer. A higher Raman shift means that compressive mean stresses are present on the surface, while a down shift is due to a tensile mean stress present at the surface. This method is very attractive

because of its potential for high spatial resolution. While during the current measurements the laser spot was about 1μm, the diameter of the focused laser beam can be as small as 150 nm (using a near-field microscope) and the penetration depth can vary from tens of nanometers to several millimeters depending on material and laser excitation wavelength. Thus, sampling a potentially large volume of the strained structure or analysis with a pin-point accuracy is possible.

Experimental technique

A Renishaw 1000 Raman microspectrometer was equipped with a Leica microscope, an XYZ mapping stage with the resolution of 0.1μm and 514.5 nm argon ion laser. The laser generated 12,5mW of power. A plasma filter was used to remove plasma lines from the spectra taken. Autofocusing was used to collect the Raman spectra because it maintains a good focus on the sample during line mapping experiments. The system was set up to take spectra from all points along a single line of interest on the surface. Line mapping of the 862 cm^{-1} Raman band of silicon nitride was performed across a 300 μm thin Si_3N_4 layer, starting from Si_3N_4-20wt%TiN layer, crossing the Si_3N_4 layer and ending in the next Si_3N_4-20wt%TiN layer. Before the Si_3N_4 measurements the spectrometer was calibrated using Si standard with Si band position at 520,3cm^{-1}.

Measurements in Si_3N_4 based laminates

The Si_3N_4/Si_3N_4-20%TiN, Si_3N_4/Si_3N_4-50%TiN, and Si_3N_4/TiN laminates, each sample having different numbers of layers and known layer thickness, were used for the calculation of the residual stresses in each layer using equations (2) and (3). The "joining" temperature, used to determine the residual stresses, was assumed to be 1200°C instead of hot pressing temperature of 1800°C. Temperature dependence of strength of these materials show that above 1200°C they are sufficiently soft to have a zero stress state due to ductile glassy phases at the grain boundaries. Results of the calculations are shown in Table 2. There exists the range of calculated residual stresses in each case because we have only approximate properties of components for our calculation. The range in Table 3 is determined with the assumption of CTE deviation ±10% from the rule of mixture.

The experimental evaluation of the sign and magnitude of residual stress by Raman spectroscopy were done and compared with the calculated data. β-Si_3N_4 belongs to the space group C^2_{6h} ($P6_3/m$) and the irreducible representation for the optical phonons has been reported

$$\Gamma_{optic} = 4A_g + 2A_u + 3B_g + 4\,B_u + 2E_{1g} + 5E_{2g} + 4E_{1u} + 2E_{2u}$$

where A_g, E_{1g} and E_{2g} modes are Raman active and A_u and E_{1u} are infrared active. Raman and infrared active bands are mutually excluded since the crystal structure has a center of symmetry.

Two typical Si_3N_4 Raman spectra are shown in Fig. 6. The spectrum in Fig. 6a was taken at the center of the thin Si_3N_4 layer of the Si_3N_4/2(Si_3N_4-20%TiN) laminate. Thickness of Si_3N_4 is about 250 μm and thickness of Si_3N_4-20%TiN layer is about 500 μm. The first indication of existing tensile mean stress came from the shift of 518 cm^{-1} position of the Si band. Free Si sometimes can be detected in Si_3N_4, as a result of desublimation of Si_3N_4. Also Si_3N_4 bands 860 cm^{-1}, 1042cm^{-1} and others are shifted to the lower wavenumbers. Three strong bands (181, 203, 224cm^{-1}), though, did not change their positions relative to the unstressed Si_3N_4. The spectrum in Fig. 6b was taken from the center of a Vickers indentation (20 kg load) placed in the center of thin Si_3N_4 layer of the same Si_3N_4/2(Si_3N_4-20%TiN) laminate. The first three bands remain intact, but the other bands shifted to the higher wave numbers. We used the published value to calculate the stress resulted from the 862 cm^{-1} band shift. Approximately 5 GPa compressive residual stress resulted from 873 cm^{-1} position in the center of the Vickers impression. Two-dimensional maps of band shift, band intensity, FWHM, and as well as other band parameters, can be produced using a line scan technique. The system is set up to take spectra from all points along a single line of interest along the surface with a given step. Line mapping of the 862 cm^{-1} Raman band of silicon nitride was performed across a thin Si_3N_4 layer in Si_3N_4/2(Si_3N_4-20%TiN) laminate, starting from Si_3N_4-20% TiN layer, crossing the interfaces and ending in the next Si_3N_4-20%TiN layer (Fig. 2). Maps of intensity (Fig. 7A), FWHM (Fig. 7B), and peak shift (Fig. 7C) were generated. As one can see, there is a shift in peak position from 862.54 cm^{-1} in Si_3N_4-20%TiN layer to 861.05 cm^{-1} in the pure Si_3N_4 layer (Fig.